Recent Advances in Nuclear Lattice Simulations

Dean Lee

Facility for Rare Isotope Beams and Department of Physics and Astronomy, Michigan State University, East Lansing, MI 48824, USA

Abstract

We review several recent results in the area of nuclear lattice simulations based on chiral effective field theory by the Nuclear Lattice EFT Collaboration. The topics we cover are lattice interactions with improved rotational properties and a computational method called eigenvector continuation.

Keywords: *Lattice simulations; effective field theory; nuclear forces; nuclear theory*

1 Introduction

Chiral effective field theory (EFT) describes the low-energy interactions of nucleons. It consists of an expansion in powers of momenta and factors of the pion mass near the chiral limit where the light quarks are massless; see Ref. [1] for a review of chiral EFT. Terms with a total of n powers of nucleon momenta or factors of the pion masses are labelled as order Q^n. The leading order (LO) interactions are at order Q^0, the next-to-leading order (NLO) interactions correspond to order Q^2, next-to-next-to-leading order (N2LO) terms are Q^3, and next-to-next-to-next-to-leading order (N3LO) are Q^4. In this Proceedings article we review two recent results using chiral EFT by the Nuclear Lattice EFT Collaboration. See also the contribution by Ulf-G. Meißner in the same Proceedings volume [2] for other recent results.

2 Improved lattice interactions

Nuclear lattice simulations using chiral EFT have been used to describe the structure and scattering of atomic nuclei [3–5]. However the treatment of nuclear forces at higher orders in the chiral expansion are difficult on the lattice due to the breaking of rotational invariance produced by the nonzero lattice spacing [6, 7].

In Ref. [8] we solve these problems with a new set of short-range chiral EFT interactions on the lattice that decomposes more easily into spin channels. The key idea is to define smeared annihilation and creation operators. This procedure gives us better rotational symmetry properties when taking spatial derivatives as finite differences. We start with $a_{i,j}(\mathbf{n})$, the nucleonic annihilation operator on lattice site $\mathbf{n}$

with spin i and isospin j. To this we add neighboring lattice operator with relative weight, s_{NL}, to define the smeared annihilation operator

$$a_{i,j}^{s_{\mathrm{NL}}}(\mathbf{n}) = a_{i,j}(\mathbf{n}) + s_{\mathrm{NL}} \sum_{|\mathbf{n}'|=1} a_{i,j}(\mathbf{n} + \mathbf{n}'). \tag{1}$$

Next we form bilinear functions of the annihilation operators with various spin and isospin quantum numbers, S, S_z, I, I_z,

$$[a(\mathbf{n})\, a(\mathbf{n}')]_{S,S_z,I,I_z}^{s_{\mathrm{NL}}} = \sum_{i,j,i',j'} a_{i,j}^{s_{\mathrm{NL}}}(\mathbf{n})\, M_{ii'}(S,S_z)\, M_{jj'}(I,I_z)\, a_{i',j'}^{s_{\mathrm{NL}}}(\mathbf{n}'). \tag{2}$$

We introduce orbital angular momentum using solid spherical harmonics,

$$R_{L,L_z}(\mathbf{r}) = \sqrt{\frac{4\pi}{2L+1}}\, r^L\, Y_{L,L_z}(\theta,\phi), \tag{3}$$

that are written as functions of the lattice derivatives of one of the annihilation operators,

$$P_{S,S_z,L,L_z,I,I_z}^{2M,s_{\mathrm{NL}}}(\mathbf{n}) = [a(\mathbf{n})\nabla_{1/2}^{2M} R_{L,L_z}^*(\nabla) a(\mathbf{n})]_{S,S_z,I,I_z}^{s_{\mathrm{NL}}}. \tag{4}$$

We then project onto the selected spin and orbital angular momentum using Clebsch–Gordan coefficients,

$$O_{S,L,J,J_z,I,I_z}^{2M,s_{NL}}(\mathbf{n}) = \sum_{S_z,L_z} \langle SS_zLL_z|JJ_z\rangle P_{S,S_z,L,L_z,I,I_z}^{2M,s_{NL}}(\mathbf{n}). \tag{5}$$

We present in Ref. [8] results for the neutron-proton system up to next-to-next-to-next-to-leading order for lattice spacings of 1.97, 1.64, 1.32, and 0.99 fm. In Fig. 1 we show results for the neutron-proton scattering phase shifts and mixing angles versus the relative momenta for the lattice spacing $a = 1.32$ fm, and in Fig. 2 we show neutron-proton scattering phase shifts and mixing angles for the lattice spacing $a = 0.99$ fm. The blue, green and red bands signify the estimated uncertainties at NLO, N2LO and N3LO respectively. The black solid line and diamonds denote phase shift or mixing angle from the Nijmegen partial wave analysis and lattice calculation at N3LO, respectively. These results show marked improvement over previous studies of chiral EFT interactions on the lattice.

3 Eigenvector continuation

In nuclear theory and other fields of quantum theory we often would like to find the extremal eigenvalues and eigenvectors of a Hamiltonian matrix in a vector space that is extremely large, so large that linear algebra operations on general vectors cannot be done. Monte Carlo methods are well suited to overcome this problem, however stochastic methods fail when severe sign oscillations appear and there is strong cancellation between positive and negative amplitudes.

We present in Ref. [9] a new technique called eigenvector continuation (EC) that can improve the reach of Monte Carlo methods. The main idea is that while an eigenvector inhabits a linear space with very many dimensions, the eigenvector trajectory generated by smooth changes of the Hamiltonian matrix can be well approximated by a low-dimensional manifold. This statement is proven using analytic continuation.
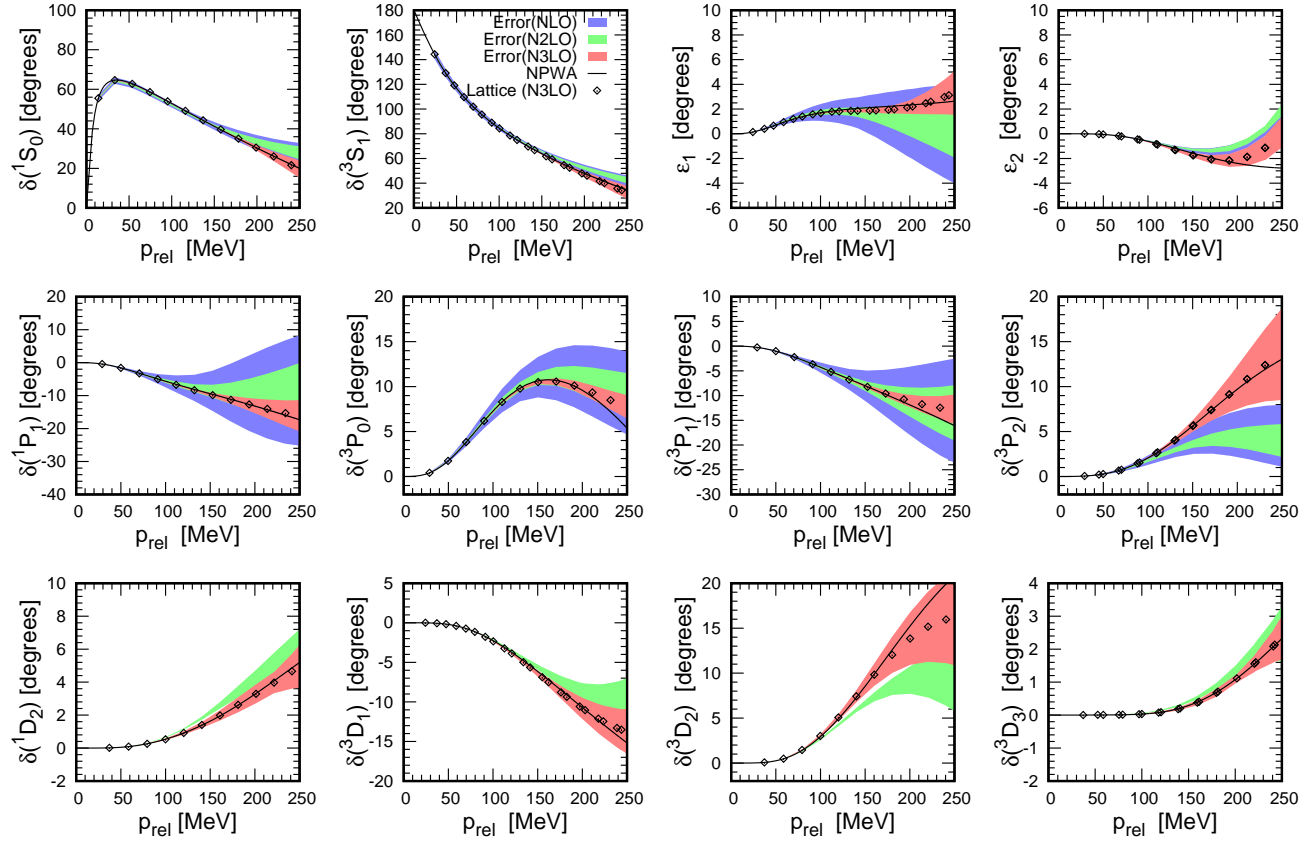
Figure 1: Results for the neutron-proton scattering phase shifts and mixing angles versus the relative momenta for the lattice spacing $a = 1.32$ fm. The blue, green and red bands signify the estimated uncertainties at NLO, N2LO and N3LO respectively. The black solid line and diamonds denote phase shifts or mixing angles from the Nijmegen partial wave analysis and lattice calculation at N3LO, respectively.
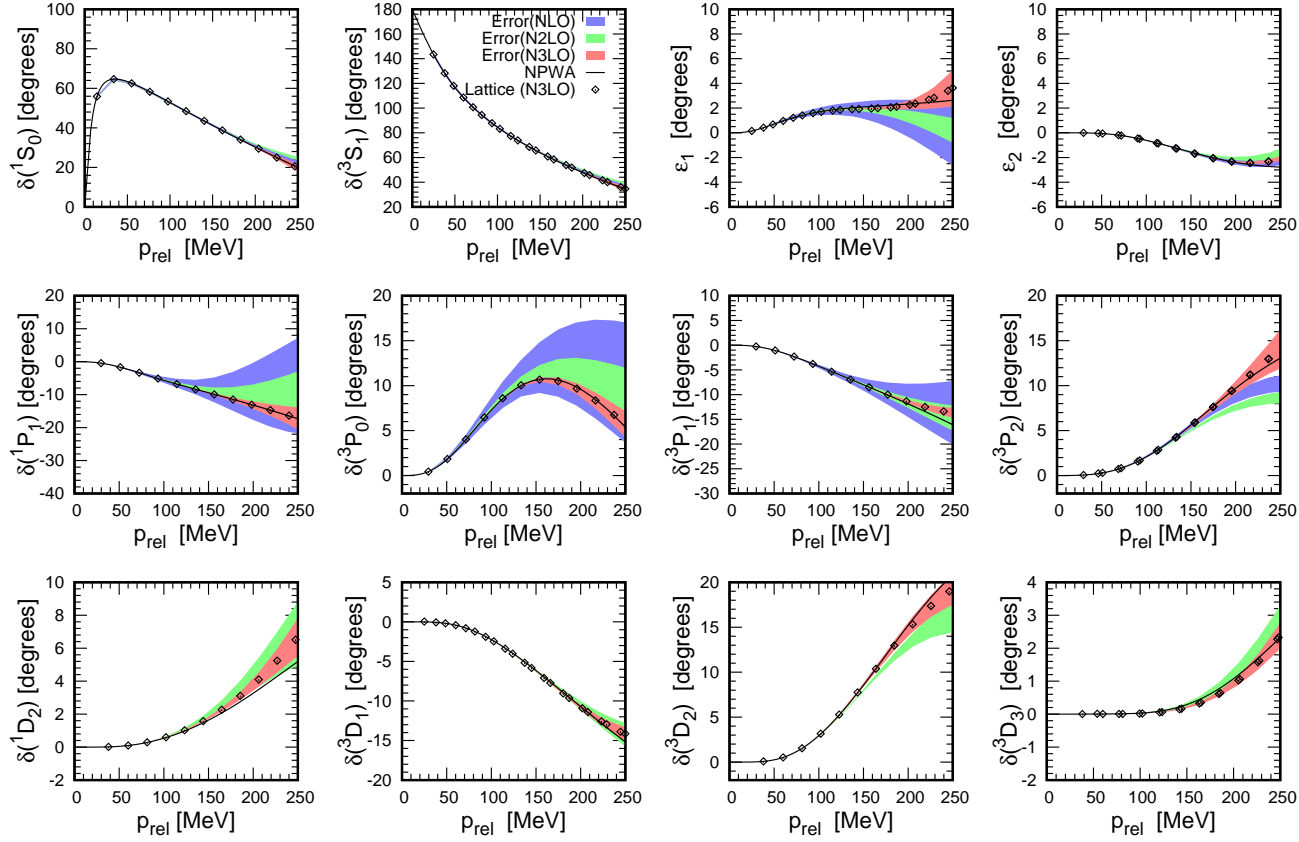
Figure 2: Results for the neutron-proton scattering phase shifts and mixing angles versus the relative momenta for the lattice spacing $a = 0.99$ fm. The blue, green and red bands signify the estimated uncertainties at NLO, N2LO and N3LO respectively. The black solid line and diamonds denote phase shifts or mixing angles from the Nijmegen partial wave analysis and lattice calculation at N3LO, respectively.

Suppose that the Hamiltonian $H(c)$ depends smoothly on some control parameter c. Let $c_\odot$ be the target value of the parameter where we wish to compute the ground state wave function $|\Psi_0(c_\odot)\rangle$. The EC method is variational calculations where the variational subspace consists of eigenvectors $|\Psi_0(c)\rangle$ for different values of c. The computational advantage is clear when the direct calculation of $|\Psi_0(c_\odot)\rangle$ is not possible but we can use values of c where the Monte Carlo simulations are accurate and reliable.

We assume that $H(c)$ is Hermitian for real c and thus diagonalizable. Hence we can define $|\Psi_0(c)\rangle$ so that it also has no singularities on the real axis. We now expand $|\Psi_0(c)\rangle$ as a power series about the point $c = 0$. The coefficients for c^n are $|\Psi_0^{(n)}(0)\rangle/n!$, where the superscript (n) indicates the nth derivative. An analogous series expansion can be applied to the eigenvalue $E_0(c)$. These series converge for all $|c| < |z|$, where z and its complex conjugate $\bar{z}$ are the closest singularities to $c = 0$ in the complex plane. Although the series expansion about $c = 0$ fails to converge for $|c| > |z|$, we can define an analytic extension by constructing a new series about another point $c = w$, where w is real and $|w| < |z|$.

For this new series the coefficients of $(c - w)^n$ are $|\Psi_0^{(n)}(w)\rangle/n!$. We can use the original series to express each $|\Psi_0^{(n)}(w)\rangle$ in terms of $|\Psi_0^{(m)}(0)\rangle$. In this way we can approximate $|\Psi_0(c)\rangle$ to arbitrary accuracy as a linear combination of the vectors $|\Psi_0^{(n)}(0)\rangle$ in the region $|c - w| < |z - w|$ centered at w. This process of analytic continuation is illustrated in Fig. 3. By applying this analytic continuation repeatedly, we can reach any value of c and express any $|\Psi_0(c)\rangle$ to any desired accuracy as a linear combination of a finite number of vectors $|\Psi_0^{(n)}(0)\rangle$. The number of required vectors is determined by the number of different expansion centers needed in the analytic continuation and the rate of convergence of each series expansion. This explains
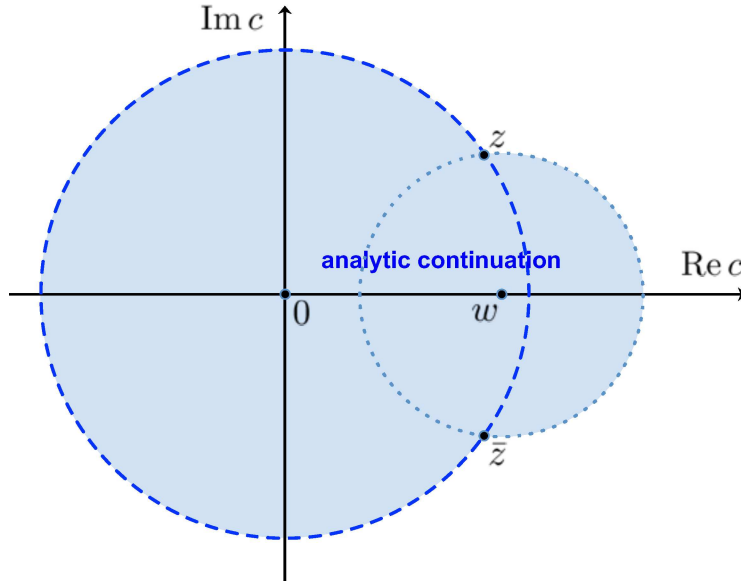

Figure 3: Analytic continuation of the wave function $|\Psi_0(c)\rangle$ beyond the nearest singularity at z and $\bar{z}$.

Table 1: EC results for the ground state energy for six and fourteen neutrons using sampling data $g_A^2 = c_1$, c_2, c_3, where $c_1 = 0.25$, $c_2 = 0.60$, and $c_3 = 0.95$. For comparison we also show the direct calculation results.

g_A^2 values	E_0, 6 neutrons (MeV)	E_0, 14 neutrons (MeV)
c_1	14.0(4)	48.8(6)
c_2	13.7(4)	48.5(7)
c_3	13.8(6)	48.8(8)
c_2, c_3	13.7(4)	48.4(7)
c_3, c_1	13.8(4)	48.8(6)
c_1, c_2	13.7(4)	48.4(7)
c_1, c_2, c_3	13.7(4)	48.4(7)
direct calculation	$12(^{+3}_{-4})$	$42(^{+7}_{-15})$

why the trajectory traced out by $|\Psi_0(c)\rangle$ can be approximated by a manifold with a small number of linearly-independent directions.

In Ref. [9] we consider simulations of the neutron matter at the leading order using the leading order interaction described in Ref. [10]. This particular lattice action is plagued by large sign oscillations due to the one-pion exchange interaction, which is parameterized by the coupling g_A^2. The systems we calculate are the ground state energies of 6 and 14 neutrons on a $4 \times 4 \times 4$ lattice with spatial lattice spacing 1.97 fm and time lattice spacing 1.32 fm. We first attempt to compute the ground state energies by direct calculation. The errors are quite large due to sign oscillations. For 6 neutrons the ground state energy is $E_0 = 12(^{+3}_{-4})$ MeV, and for 14 neutrons $E_0 = 42(^{+7}_{-15})$ MeV.

Next we use the EC for the values $g_A^2 = c_1$, c_2, c_3, where $c_1 = 0.25$, $c_2 = 0.60$, and $c_3 = 0.95$. We use Monte Carlo simulations to calculate the ground state eigenvectors for c_1, c_2, c_3. In Table 1 we show the EC results using just one of the three vectors, two of the vectors, or all three vectors. The error bars are estimates of the stochastic error and extrapolation error in the projection time. For comparison we also show the direct calculation results. The EC results are consistent with the direct calculation results, though with an error bar that is smaller by an order of magnitude. The EC approach is now being developed for all interactions that produce sign oscillations in the nuclear lattice simulations.

4   Acknowledgements

References

[1] E. Epelbaum, H. W. Hammer and U.-G. Meißner, Rev. Mod. Phys. **81**, 1773 (2009).

[2] U.-G. Meißner, *see these Proceedings*, p. 28, http://www.ntse.khb.ru/files/uploads/2018/proceedings/Meissner.pdf.

[3] E. Epelbaum, H. Krebs, D. Lee and U.-G. Meißner, Phys. Rev. Lett. **106**, 192501 (2011).

[4] E. Epelbaum, H. Krebs, T. A. Lähde, D. Lee and U.-G. Meißner, Phys. Rev. Lett. **109**, 252501 (2012).

[5] S. Elhatisari, D. Lee, G. Rupak, E. Epelbaum, H. Krebs, T. A. Lähde, T. Luu and U.-G. Meißner, Nature **528**, 111 (2015).

[6] J. M. Alarcón *et al.*, Eur. Phys. J. A **53**, 83 (2017).

[7] N. Klein, S. Elhatisari, T. A. Lähde, D. Lee and U.-G. Meißner, Eur. Phys. J. A **54**, 121 (2018).

[8] N. Li, S. Elhatisari, E. Epelbaum, D. Lee, B. N. Lu and U.-G. Meißner, Phys. Rev. C **98**, 044002 (2018).

[9] D. Frame, R. He, I. Ipsen, D. Lee, D. Lee and E. Rrapaj, Phys. Rev. Lett. **121**, 032501 (2018).

[10] D. Lee, Lecture Notes Phys. **936**, 237 (2017).